


# Carrier transport after ultrashort-pulse laser excitation in dielectric materials leads to 10 MV m<sup>-1</sup> electric fields: Transient birefringence and emission of terahertz radiation

Søren H. Møller <sup>\*</sup>, Peter S. Sneftrup , Brian Julsgaard, and Peter Balling <sup>†</sup>

Department of Physics and Astronomy, Aarhus University, Ny Munkegade 120, 8000 Aarhus C, Denmark

 (Received 25 February 2023; revised 21 February 2024; accepted 25 March 2024; published 17 April 2024)

Charge-carrier transport is investigated theoretically in a high-band-gap dielectric material excited by intense ultrashort laser pulses. Simulations of fused silica reveal that the photo-Dember effect causes a 10<sup>7</sup> Vm<sup>-1</sup> electric field to build up inside the material. It is shown that this electric field can induce a significant transient optical anisotropy in the dielectric, which may help reconcile earlier reports of an ultrafast onset of birefringence in highly excited fused silica. The time-dependent electric field will also lead to emission of a broadband THz pulse propagating out from and along the dielectric surface.

DOI: [10.1103/PhysRevB.109.L140304](https://doi.org/10.1103/PhysRevB.109.L140304)

*Introduction.* The sudden generation of electron-hole pairs near the surface of a band-gap material by a light pulse sets up a transient electric field perpendicular to the surface. This phenomenon, the photo-Dember effect [1,2], results from a difference in electron and hole mobilities: The typically more mobile electrons diffuse into the bulk of the material, leaving a positive electric charge at the surface. This in turn generates an electric field directed into the bulk that slows down the electron diffusion and speeds up the holes. The electric field, henceforth referred to as the *Dember field*, persists until the electron-hole transport has terminated.

In semiconductors, the transient Dember field is widely exploited in the generation of THz radiation [3–7]. However, in the context of dielectrics, the photo-Dember effect is rarely discussed, possibly because of their much lower electron and hole mobilities compared to semiconductors, yet this overlooks the fact that the Dember field depends on the *relative difference* in electron and hole mobilities. Furthermore, the ultrafast excitation of a dielectric has several properties that could enhance the Dember field: The extremely nonlinear photoexcitation process in dielectrics requires high intensities to initiate strong-field excitation [8]. The electrons excited to the conduction band are subsequently heated to large temperatures by the laser pulse, multiplying the conduction-band electron density by collisional excitation [9,10]. This rapid increase in the electron-hole density shields the tail of the laser pulse, leading to very steep density gradients and high carrier temperatures [11,12], both of which will reinforce the photo-Dember effect.

In this Letter, we show through detailed simulations that the induced Dember field in highly excited dielectrics reaches magnitudes of 10<sup>7</sup> Vm<sup>-1</sup>. The large Dember field has an interesting consequence for the ensuing electron-hole dynamics: It distorts the electron-hole distribution in reciprocal space (*k* space) and may induce a transient electro-optical anisotropy

in materials with nonparabolic conduction and/or valence bands, thus possibly explaining prior observations of transient birefringence in fused silica excited by an ultrashort laser pulse [13]. We also calculate that a strong THz pulse is emitted from and along the dielectric surface.

*Simple physical picture.* Consider the generation of an electron-hole pair near the surface of a band-gap material in a one-dimensional model, where transport proceeds along *z*, perpendicular to the surface. The carrier concentrations are denoted *N<sub>i</sub>*, where *i* stands for either *e* (electrons) or *h* (holes). Assuming for now, for simplicity, that the charge carriers are nondegenerate, the charge-current density is

$$J_i = -(q_i/e)\mu_i k_B T_i \nabla N_i + e\mu_i N_i E_D, \quad (1)$$

where the first term represents diffusion ( $\nabla = \partial/\partial z$ ) and the last term represents drift in the Dember field  $E_D$ . Note that  $q_e = -e$ , and  $q_h = e$ . If the charge densities are sufficiently large,  $E_D$  will ensure that the electrons and holes move together and the total current cancels:  $J_e + J_h = 0$ . This is the condition for ambipolar diffusion. Assuming  $N_e \approx N_h$  and  $T_e \approx T_h$  leads to the simple expression for the ambipolar electric field [2]:

$$E_D = \frac{k_B T}{e} \left( \frac{\mu_h - \mu_e}{\mu_h + \mu_e} \right) \frac{\nabla N}{N}. \quad (2)$$

According to the semiclassical model in solids [14], the crystal momentum imparted to an electron by the Dember field (directed along *z*) is

$$k_z(t) = -\frac{e}{\hbar} \int_{-\infty}^t dt' E_D(t') e^{-(t-t')/\tau_M}. \quad (3)$$

Here,  $\tau_M$  is the mean electron-momentum relaxation time. As a result, the electron-hole distributions are displaced in *k* space as sketched in Fig. 1. If the change in *k* is a significant fraction of the size of the first Brillouin zone, the optical response of electrons displaced in the direction of  $E_D$  may change significantly. This can be seen by considering the nonparabolic band structure  $\epsilon^k(1 + \alpha\epsilon^k) = \hbar^2 k^2/2m$ : The effective mass  $m_{ab}^{-1} = \hbar^{-2} \partial^2 \epsilon^k / \partial k_a \partial k_b$  now depends on **k**. When

<sup>\*</sup>soerenhm@phys.au.dk

<sup>†</sup>balling@phys.au.dk

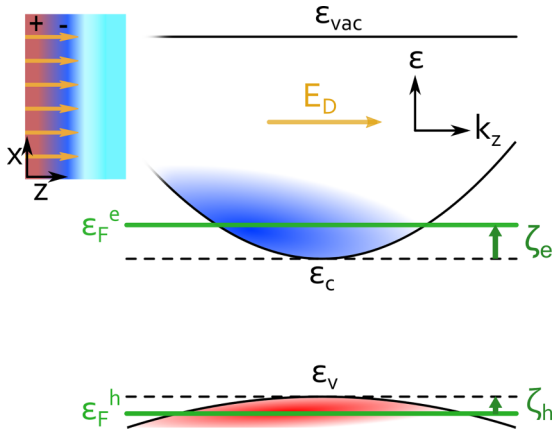


FIG. 1. Electron (blue) and hole (red) distributions in  $k$  space, distorted by the Dember field  $E_D$ . Energies are measured from the vacuum level  $\epsilon_{\text{vac}}$  while the quasichemical potentials  $\zeta_i$  are measured from (to) the band edges for electrons (holes). The upper left inset shows the charge-density distribution at the dielectric surface (left) that creates the Dember field.

$k_x \approx k_y \approx 0$ , the ratio between the effective mass in  $z$  and in  $x$  (or  $y$ ) is  $m_{zz}/m_{xx} = 1 + 2\alpha\hbar^2 k_z^2/m$ . Anisotropy emerges because  $m_{zz}$  increases more rapidly with  $k_z$  (or decreases if  $\alpha < 0$ ), an effect which was observed in a THz pump-probe experiment on  $n$ -doped InGaAs thin films [15].

From Eq. (2) we can estimate the order of magnitude of the Dember field. Consider InAs, an excellent emitter of THz radiation by the photo-Dember effect. It has a high electron mobility of  $\mu_e = 4 \times 10^4 \text{ cm}^2 \text{ V}^{-1} \text{ s}^{-1}$  and short absorption length: about 150 nm for excitation with 800 nm light, with excess electron energies of 0.5 eV [16]. Thus  $\nabla N/N = 6.7 \times 10^6 \text{ m}^{-1}$ ,  $k_B T/e = 0.5 \text{ V}$ , leading to a Dember field of  $E_D = 3 \times 10^6 \text{ Vm}^{-1}$ .

Note that the Dember field according to Eq. (2) does not depend on the carrier density, only the carrier-density gradient, which, to first order, does not change with an increasing fluence for direct photon absorption.

In wide-band-gap dielectric materials, where multiple photons are needed to bridge the band gap (nominally six 1.5 eV photons for SiO<sub>2</sub>), light absorption proceeds through strong-field excitation [8]. This creates the initial seed of electron-hole pairs, while the subsequent heating of the carriers to very high temperatures by the trailing edge of the laser pulse initiates collisional excitation, drastically increasing the electron-hole pair density [9,10]. This nonlinear excitation process results in very steep gradients in the electron-hole density, leading to density gradients with length scales of the order 10–100 nm [11–13] while electron temperatures easily reach  $10^4 \text{ K}$ . With  $\mu_e \approx 10\mu_h$ , Eq. (2) predicts that the Dember field ranges from  $10^7$  to  $10^8 \text{ Vm}^{-1}$ —this is larger than  $E_D$  in InAs, a state-of-the-art THz emitter. Moreover, the Dember field displaces the electron-hole distribution in  $k$  space;  $\Delta k \approx 10^9 \text{ m}^{-1}$  according to Eq. (3), assuming an electron-momentum relaxation time of 100 fs. This displacement in  $k$  space is comparable to the size of the Brillouin zone, and therefore significant birefringence is expected.

*Transport model.* Equation (2) shows that the magnitude of the Dember field is directly proportional to the temperature. This was derived for a nondegenerate electron-hole distribution; a proper description must consider the combined flow of charge and kinetic energy that is valid also for a degenerate electron-hole distribution. For simplicity, we assume that the laser-excited electrons and holes thermalize in their respective bands instantly during laser excitation so that their distribution functions can be represented by quasi-Fermi energies  $\epsilon_F^i$  and temperatures  $T_i$ . Following Ref. [17], the kinetic (or internal) energy-current density  $u_i$  and charge-current density  $J_i$  are expressed as

$$u_i = -L_{11}^i \nabla T_i / T_i + L_{12}^i \nabla \epsilon_F^i / e, \quad (4a)$$

$$J_i = -L_{21}^i \nabla T_i / T_i + L_{22}^i \nabla \epsilon_F^i / e. \quad (4b)$$

The coefficients  $L_{ab}^i$  are functions of  $T_i$  and  $\epsilon_F^i$  and are determined from the band structure (for details, see Supplemental Material [18]). The quasi-Fermi energy is the sum of the quasichemical potential  $\zeta_i$  and the electrostatic potential  $\phi$  induced by the Dember field ( $E_D = -\nabla\phi$ ), thus  $\nabla \epsilon_F^e = \nabla \zeta_e + eE_D$  and  $\nabla \epsilon_F^h = -\nabla \zeta_h + eE_D$  (see Fig. 1 for the sign convention). Band-gap narrowing, which may be several eV for carrier concentrations approaching  $10^{28} \text{ m}^{-3}$  [19–21], can be included as an additional potential; however, first-principles calculations show that band-gap narrowing in  $\alpha$ -quartz depends mainly on carrier temperature [22], which turns out to have small spatial gradients in our case, hence this effect is ignored. Energy transport due to phonons is also not included since this is negligible on the ultrafast timescales that we consider here.

The current-density equations are related to continuity equations for the kinetic (internal) energy density  $U_i$  and number density  $N_i$  as [17,23]

$$\frac{\partial U_i}{\partial t} = -\nabla \cdot u_i + E_D \cdot J_i + H_i - \mathcal{L}_{\text{ph}}^i - \mathcal{L}_{\text{eh}}^i, \quad (5a)$$

$$\frac{\partial N_i}{\partial t} = -\frac{1}{q_i} \nabla \cdot J_i + G_i. \quad (5b)$$

The terms  $\mathcal{L}_{\text{ph}}^i$  and  $\mathcal{L}_{\text{eh}}^i$  represent energy losses due to inelastic phonon scattering and electron-hole thermalization;  $H_i$  and  $G_i$  are the source terms of internal energy and carriers from the photoexcitation process. The Dember field  $E_D$  is obtained from Ampère's law:

$$\frac{\partial E_D}{\partial t} = -\frac{1}{\epsilon_0 \epsilon_\infty} (J_e + J_h). \quad (6)$$

*Simulations of fused silica.* We calculate the photo-Dember field in fused silica after excitation with an ultrashort laser pulse. The band structure of the amorphous material is not known, however it has been argued that it resembles the crystalline structures of SiO<sub>2</sub> ( $\alpha$ -quartz and  $\beta$ -cristobalite) with effective mass  $m_c = 0.5m_e$  in the conduction band [24] and  $m_v \approx 10m_e$  in the valence band [25–27], and  $\epsilon_\infty = 3.8$ . To investigate the effects of anisotropy induced by the Dember field, we assume a nonparabolicity of  $\alpha = 2 \text{ eV}^{-1}$ . Reported electron mobilities of fused silica vary widely [28]. We assume a reasonable electron-momentum relaxation time  $\tau_M$  of 120 fs [29], chosen also because it provides a good match with experimental data discussed later. The resulting electron

mobility is  $420 \text{ cm}^2 \text{ V}^{-1} \text{ s}^{-1}$ , which we note is about 20 times larger than measured [30] and calculated [24] values, obtained for low carrier concentrations. In a highly excited dielectric, carrier screening could significantly reduce or saturate carrier-phonon interactions, leading to higher mobilities.

Under ambipolar diffusion, which can be established on ultrafast timescales for high excitation densities, mainly the least mobile charge carrier (here, holes) determines the diffusion time because the Dember field forces the electrons and holes to move together. Since no evidence of significant carrier diffusion appears in the time-resolved data in fused silica discussed later, we set  $\mu_h = 2.1 \text{ cm}^2 \text{ V}^{-1} \text{ s}^{-1}$ , but any lower value is also consistent with the observed timescales.

Carrier-phonon coupling is expressed as  $\mathcal{L}_{\text{ph}}^i = g_{\text{ph}}^i (T_i - 300 \text{ K})$  and electron-hole coupling as  $\mathcal{L}_{\text{eh}}^i = g_{\text{eh}}^i \Delta T_i$  ( $\Delta T_e = T_e - T_h$  for electrons;  $\Delta T_h = T_h - T_e$  for holes). The coupling constants are approximated as  $g^i = C_i/\tau$  where  $C_i$  is the heat capacity and  $\tau$  is a thermalization time [31]. Electron-hole thermalization is fast:  $\tau_{\text{eh}} = 10 \text{ fs}$  [32]. From the computed electron-phonon coupling strength in Ref. [33] we estimate that  $\tau_{\text{ph}}^i \approx 10 \text{ ps}$  under the assumption that  $C_i \approx \frac{3}{2} k_B T_i N_i$ .

The density and temperature distributions of the electrons and holes are obtained from the multiple-rate-equation (MRE) model for excitation of dielectrics [9,26,27] coupled with finite-difference time-domain simulations of ultrashort-pulse propagation in the excited material [34]—for more details, see Supplemental Material [18]. To mimic the experimental conditions in Ref. [13], we excite fused silica with a 35 fs temporally Gaussian laser pulse centered at 800 nm with a fluence of  $2.6 \text{ J cm}^{-2}$ . The electron-hole density  $N$  and their temperatures ( $T_e, T_h$ ) immediately after excitation are displayed in Fig. 2(a). The kink in the Dember field magnitude at a depth of  $\sim 380 \text{ nm}$  stems from a small increase in the carrier density (barely visible in the figure), which originates from the MRE simulations and reflects the effect of the ponderomotive energy shift of the band gap on the excitation.

The initial steep density gradients lead to fast diffusion, which quickly builds up the Dember field  $E_D$ . At the surface,  $E_D$  rises to  $5 \times 10^6 \text{ Vm}^{-1}$  and reaches  $8 \times 10^6 \text{ Vm}^{-1}$  a few nm from the surface as shown in Fig. 2(b). The Dember field subsequently follows the motion of hot carriers into the bulk, which causes a fast decrease in  $E_D$  at the surface: After 2 ps, the peak of  $E_D$  has moved 20 nm into the bulk. The electrons and holes thermalize to a common temperature of 17 000 K about 10 fs after excitation, and then cool very slowly because of diffusion and energy transfer to the lattice [Fig. 2(c)]. We have not included the effect of hot-electron emission from the solid. This effect would increase  $E_D$  at the surface, and could lead to Coulomb explosion of a thin surface layer [35], however the simulated carrier temperatures are too low for this to be a significant effect.

Using Eq. (3), we calculate the crystal momentum  $k_z$  imparted to electrons by the Dember field assuming  $\tau_M = 120 \text{ fs}$ . The crystal momentum versus depth from the surface and time is shown in Fig. 3(a). Near the surface,  $k_z$  increases to about 25% of the size of the Brillouin zone ( $k_{\text{BZ}} = \pi/4.9 \text{ \AA}$ ). The resulting time-dependent effective masses in  $z$  and  $x$ , averaged over 20 nm from the surface, are displayed in Fig. 3(b):  $m_{zz}$  increases by a factor 3;  $m_{xx}$  increases only slightly.

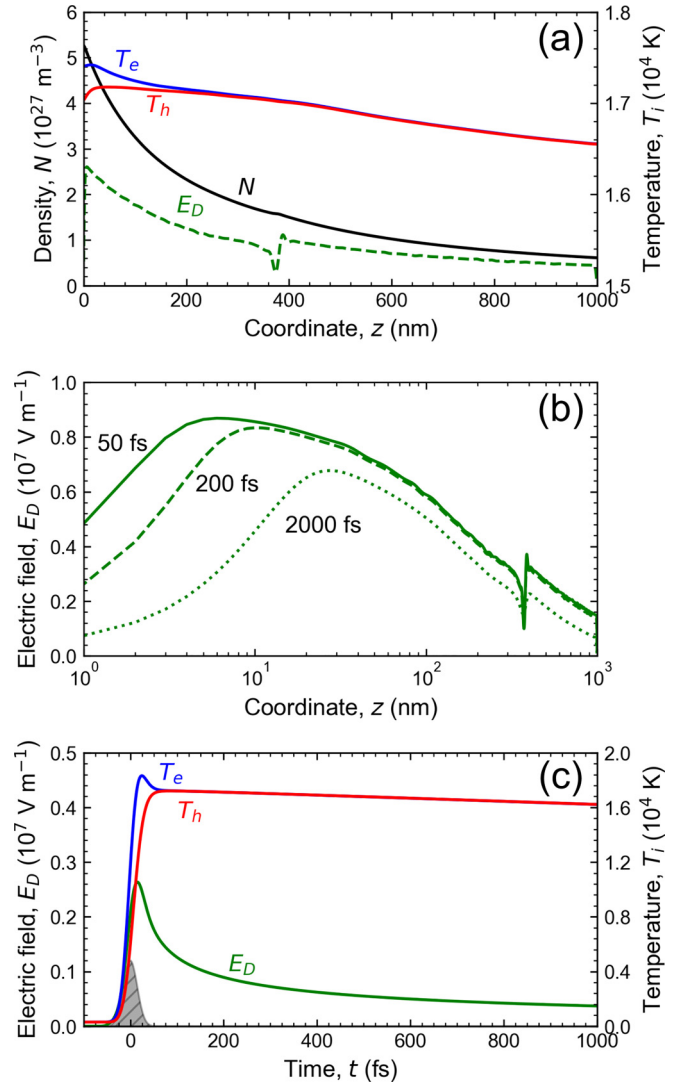


FIG. 2. (a) Simulated initial number densities and temperatures of electrons ( $N_e, T_e$ ) and holes ( $N_h, T_h$ ) at  $t = 50 \text{ fs}$ . Note that  $N_e \approx N_h = N$  in this case. The dashed green curve shows, in relative units, the spatial profile of the Dember field  $E_D$ . (b) Spatial profile of the photo-Dember field on a logarithmic depth scale at selected times after excitation. (c) Time evolution of the temperatures and the Dember field at the surface ( $z = 0$ ). The shaded area centered at time zero illustrates the intensity envelope of the excitation laser pulse.

The time-dependent anisotropic effective masses change the optical response of the electron-hole plasma. In Ref. [13], based on time-resolved reflectivity measurements of  $R_p$  and  $R_s$  of strong-laser-pulse excited fused silica, it was concluded that a transient birefringence was necessary to explain the measurements. In Fig. 3(c), measurements performed at 700 nm and  $60^\circ$  angle of incidence are reproduced from Ref. [13]. The solid lines are reflectivity calculations based on a Drude model [36] (for details, see Supplemental Material [18]) using the time-dependent effective masses in Fig. 3(b) and assuming a constant Drude scattering rate of  $\Gamma = 1.6 \times 10^{15} \text{ s}^{-1}$ . The calculated curves were convolved with a Gaussian kernel of 125 fs full width at half maximum to reproduce the slow buildup of the reflectivity, often

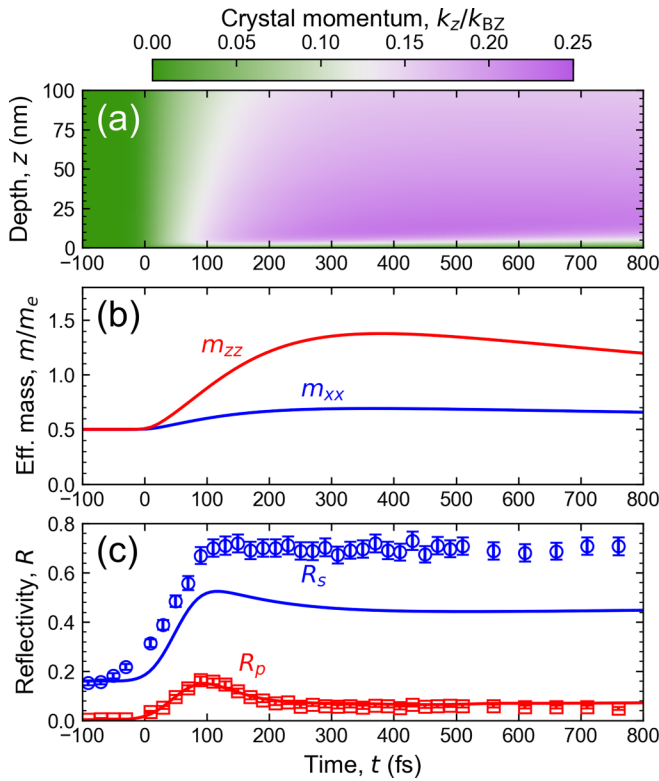


FIG. 3. Simulated effects of the Dember field on electrons in laser-excited fused silica. (a) Crystal momentum imparted to an electron at time  $t$  at a depth  $z$  from the surface with  $\tau_M = 120$  fs. (b) Time-dependent effective mass along  $z$  ( $m_{zz}$ ) and  $x$  ( $m_{xx}$ ), averaged over a 20 nm depth from the surface. (c) Transient reflectivities of  $p$ - and  $s$ -polarized light ( $R_p$  and  $R_s$ ) for a 700 nm probe pulse incident at  $60^\circ$  to the surface. Measurements are from Ref. [13]; solid lines are calculations based on the model presented in the main text.

observed in such experiments [13,37]. The transient increase in effective electron-hole masses reproduces the ultrafast drop in  $R_p$  well, however the calculated  $R_s$  is too low compared to the measurements; most likely the assumed band structure does not accurately represent fused silica. Nevertheless, our calculations show that the photo-Dember effect can have a huge impact on the optical response through an induced optical anisotropy. This significant effect has, to our knowledge, previously been overlooked.

The transient Dember field also leads to emission of THz radiation from the surface. We can treat the induced charge-current density as a dipole source, since the wavelength of the radiation is very large. The radiated electric field at a distance  $r$  from the current-element source in the direction  $\theta$  from  $z$  is  $E(r, \theta, t) = (4\pi\epsilon_0rc^2)^{-1} \sin\theta \int (dJ(z, t)/dt) dV$  [38], where the integration is over the laser-excited volume. Figure 4(a) shows the radiated field integrated over  $z$  and normalized to the cross-sectional area  $A$  of the laser spot and the inverse distance ( $1/r$ ) to the source. The radiation builds up rapidly during the laser pulse due to fast diffusion of newly generated electrons and holes. The spike around  $t = 50$  fs is caused by the slowing down of electrons due to the rapid buildup of the Dember field. Because of the high excitation density, ambipolar diffusion is established immediately after the laser

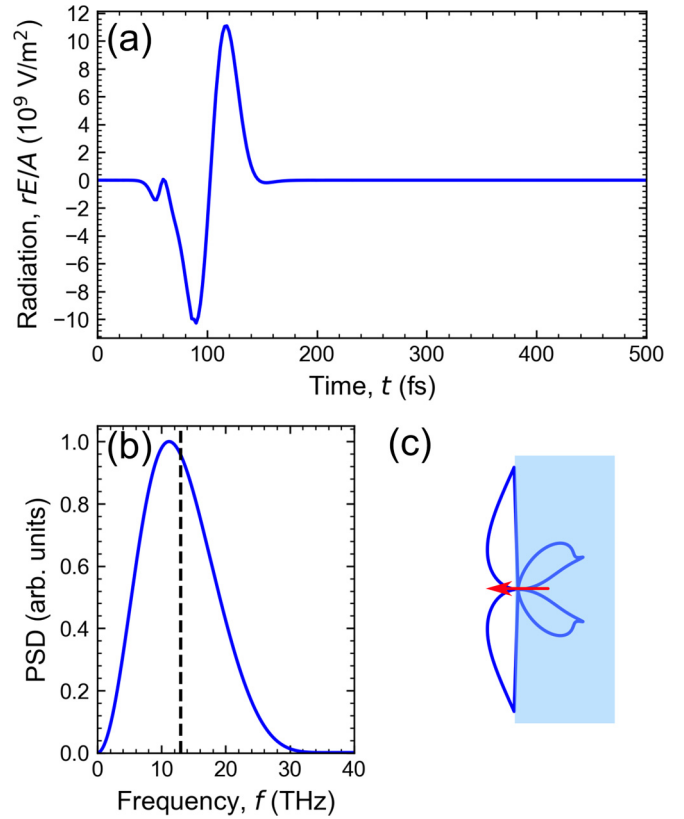


FIG. 4. THz pulse emitted from fused silica. (a) Instantaneous electric-field strength in the far field, and (b) the associated power-spectral density (PSD). The peak of the 35 fs pump pulse strikes the material surface at  $t = 105$  fs. (c) Polar plot of the emitted THz electric-field magnitude from the sample surface. The blue-shaded area represents the solid. The red arrow marks the direction of the transient photo-Dember current.

pulse excitation, i.e., at around  $t = 140$  fs, which leads to a saturation of the achievable THz pulse energy (see Fig. 2 in Supplemental Material [18]), at around  $2.2 \times 10^4$  J/m<sup>4</sup>. To put this number in perspective, imagine that the excitation laser pulse of  $2.6$  J cm<sup>-2</sup> has a beam radius of  $100$   $\mu$ m: The THz pulse energy is then about 22 pJ, which is easily measurable using standard electro-optic sampling.

We remark that the high laser fluence, considered here, leads to ablation of the material. Motion of ions and possibly excitation of coherent phonons could contribute to the THz radiation. However, prior studies on laser ablation of fused silica have found no significant ion motion before at least 3 ps [39]. Therefore, THz radiation due to ion motion is probably a small effect and is neglected in our model.

The estimated THz energy of  $2.2 \times 10^4$  J/m<sup>4</sup> here achieved at  $2.2$  J m<sup>-2</sup> is, according to simulations of the photo-Dember effect in InAs, achieved already at approximately 100 times lower fluence [6]. This is not so surprising as the process in SiO<sub>2</sub> is based on strong-field excitation.

The dependence of radiated THz pulse energy on the laser fluence is complicated, as the photo-Dember electric field magnitude depends on the *gradient* of the electron-hole density and their temperatures [Eq. (2)]. At increasingly higher laser fluences, the electron-hole temperatures



saturate due to avalanche ionization, where hot electrons and holes cool by creation of additional carriers through impact ionization.

The power-spectral density (PSD) of the THz pulse is displayed in Fig. 4(b), where the mean frequency of  $\sim 11$  THz is highlighted (dashed line). The high THz-pulse bandwidth is a consequence of the rapid growth of the Dember field given by the laser-pulse excitation bandwidth of the densities; at very short-pulse durations (10 fs), the THz bandwidth drops below this limit, possibly due to the finite electron mobility (Fig. 2 in Supplemental Material [18]). Part of the radiation undergoes total internal reflection at the interface with air because of the high refractive index at THz frequencies, 2.26 at 6 THz [40]. The far-field THz radiation pattern is shown in Fig. 4(c). The total internally reflected wave cancels part of the radiation

emitted inside and close to parallel with the solid surface, and produces evanescent THz waves propagating along the dielectric surface.

*Summary.* We have shown that the photo-Dember effect in highly excited dielectric materials leads to broadband THz radiation and that it, for nonparabolic band structures, induces significant optical birefringence, despite the very low electron-hole mobilities in dielectric materials. The optical birefringence is a signature of the charge carriers moving through the band structure under the electric field caused by the photo-Dember effect, which can serve as an experimental probe of the internal electron-hole dynamics [41,42].

*Acknowledgment.* This work was supported by Independent Research Fund Denmark Natural Sciences.

- 
- [1] H. Dember, Über eine photoelektronische Kraft in Kupferoxydul-Kristallen (Photoelectric E.M.F. in Cuprous-Oxide Crystals), *Phys. Z.* **32**, 554 (1931).
- [2] P. Würfel and U. Würfel, *Physics of Solar Cells: From Basic Principles to Advanced Concepts* (Wiley, Hoboken, NJ, 2016).
- [3] T. Dekorsy, T. Pfeifer, W. Kütt, and H. Kurz, Subpicosecond carrier transport in GaAs surface-space-charge fields, *Phys. Rev. B* **47**, 3842 (1993).
- [4] M. B. Johnston, D. M. Whittaker, A. Corchia, A. G. Davies, and E. H. Linfield, Simulation of terahertz generation at semiconductor surfaces, *Phys. Rev. B* **65**, 165301 (2002).
- [5] J. N. Heyman, N. Coates, A. Reinhardt, and G. Strasser, Diffusion and drift in terahertz emission at GaAs surfaces, *Appl. Phys. Lett.* **83**, 5476 (2003).
- [6] A. Reklaitis, Terahertz emission from InAs induced by photo-Dember effect: Hydrodynamic analysis and Monte Carlo simulations, *J. Appl. Phys.* **108**, 053102 (2010).
- [7] G. Klatt, F. Hilser, W. Qiao, M. Beck, R. Gebbs, A. Bartels, K. Huska, U. Lemmer, G. Bastian, M. Johnston, M. Fischer, J. Faist, and T. Dekorsy, Terahertz emission from lateral photo-Dember currents, *Opt. Express* **18**, 4939 (2010).
- [8] L. V. Keldysh, Ionization in the field of a strong electromagnetic wave, *Sov. Phys. JETP* **20**, 1307 (1965).
- [9] B. Rethfeld, Free-electron generation in laser-irradiated dielectrics, *Phys. Rev. B* **73**, 035101 (2006).
- [10] P. Balling and J. Schou, Femtosecond-laser ablation dynamics of dielectrics: Basics and applications for thin films, *Rep. Prog. Phys.* **76**, 036502 (2013).
- [11] S. Guizard, A. Semerok, J. Gaudin, M. Hashida, P. Martin, and F. Quéré, Femtosecond laser ablation of transparent dielectrics: Measurement and modelisation of crater profiles, *Appl. Surf. Sci.* **186**, 364 (2002).
- [12] K. Wædegaard, D. B. Sandkamm, L. Haahr-Lillevang, K. G. Bay, and P. Balling, Modeling short-pulse laser excitation of dielectric materials, *Appl. Phys. A* **117**, 7 (2014).
- [13] S. H. Møller, S. T. Andersen, and P. Balling, Transient optical properties of highly excited dielectric materials: Apparent birefringence and delayed reflectivity increase, *Phys. Rev. Res.* **2**, 043010 (2020).
- [14] N. W. Ashcroft and N. D. Mermin, *Solid State Physics* (Brooks/Cole, Belmont, CA, 1976).
- [15] F. Blanchard, D. Golde, F. H. Su, L. Razzari, G. Sharma, R. Morandotti, T. Ozaki, M. Reid, M. Kira, S. W. Koch, and F. A. Hegmann, Effective mass anisotropy of hot electrons in nonparabolic conduction bands of *n*-doped InGaAs films using ultrafast terahertz pump-probe techniques, *Phys. Rev. Lett.* **107**, 107401 (2011).
- [16] X.-C. Zhang and J. Xu, *Introduction to THz Wave Photonics* (Springer, New York, 2010), Vol. 29.
- [17] J. Parrott, Thermodynamic theory of transport processes in semiconductors, *IEEE Trans. Electron Devices* **43**, 809 (1996).
- [18] See Supplemental Material at <http://link.aps.org/supplemental/10.1103/PhysRevB.109.L140304> for more details about the numerical model and additional figures on the space-time evolution of the Dember field and electron-hole properties; and on the THz-pulse energy and frequency scaling with the electron-hole excitation density.
- [19] T. Winkler, L. Haahr-Lillevang, C. Sarpe, B. Zielinski, N. Götte, A. Senftleben, P. Balling, and T. Baumert, Laser amplification in excited dielectrics, *Nat. Phys.* **14**, 74 (2018).
- [20] T. Winkler, P. Balling, B. Zielinski, C. Sarpe, N. Jelzow, R. Ciobotea, A. Senftleben, and T. Baumert, Unveiling nonlinear regimes of light amplification in fused silica with femtosecond imaging spectroscopy, *Phys. Rev. Res.* **2**, 023341 (2020).
- [21] A. Tsaturyan, E. Kachan, R. Stoian, and J.-P. Colombier, Ultrafast bandgap narrowing and cohesion loss of photoexcited fused silica, *J. Chem. Phys.* **156**, 224301 (2022).
- [22] E. Kachan, A. Tsaturyan, R. Stoian, and J.-P. Colombier, First-principles study of ultrafast bandgap dynamics in laser-excited  $\alpha$ -quartz, *Eur. Phys. J.: Spec. Top.* **232**, 2241 (2023).
- [23] J. E. Parrott, Transport theory of semiconductor energy conversion, *J. Appl. Phys.* **53**, 9105 (1982).
- [24] W. Porod and D. K. Ferry, Monte Carlo study of high-energy electrons in silicon dioxide, *Phys. Rev. Lett.* **54**, 1189 (1985).
- [25] M. I. Vexler, S. E. Tyaginov, and A. F. Shulekin, Determination of the hole effective mass in thin silicon dioxide film by means of an analysis of characteristics of a MOS tunnel emitter transistor, *J. Phys.: Condens. Matter* **17**, 8057 (2005).

- [26] B. H. Christensen and P. Balling, Modeling ultrashort-pulse laser ablation of dielectric materials, *Phys. Rev. B* **79**, 155424 (2009).
- [27] M. Garcia-Lechuga, L. Haahr-Lillevang, J. Siegel, P. Balling, S. Guizard, and J. Solis, Simultaneous time-space resolved reflectivity and interferometric measurements of dielectrics excited with femtosecond laser pulses, *Phys. Rev. B* **95**, 214114 (2017).
- [28] W.-Q. Li and H.-B. Zhang, The positive charging effect of dielectric films irradiated by a focused electron beam, *Appl. Surf. Sci.* **256**, 3482 (2010).
- [29] E. J. Yoffa, Dynamics of dense laser-induced plasmas, *Phys. Rev. B* **21**, 2415 (1980).
- [30] R. C. Hughes, Charge-carrier transport phenomena in amorphous Si: Direct measurement of the drift mobility and lifetime, *Phys. Rev. Lett.* **30**, 1333 (1973).
- [31] B. Rethfeld, A. Ramer, N. Brouwer, N. Medvedev, and O. Osmani, Electron dynamics and energy dissipation in highly excited dielectrics, *Nucl. Instrum. Methods Phys. Res. Sect. B* **327**, 78 (2014).
- [32] A. Ramer, Excitation and relaxation dynamics in laser-excited semiconductors and dielectrics, Ph.D. thesis, Fachbereich Physik, TU Kaiserslautern, 2017.
- [33] N. Brouwer and B. Rethfeld, Excitation and relaxation dynamics in dielectrics irradiated by an intense ultrashort laser pulse, *J. Opt. Soc. Am. B* **31**, C28 (2014).
- [34] P. S. Sneftrup, S. H. Moller, and P. Balling, Model of ultrashort-pulse laser excitation of bulk and thin film dielectrics: Coupling material excitation and electric field propagation, *Phys. Rev. B* **108**, 094307 (2023).
- [35] R. Stoian, A. Rosenfeld, D. Ashkenasi, I. V. Hertel, N. M. Bulgakova, and E. E. B. Campbell, Surface charging and impulsive ion ejection during ultrashort pulsed laser ablation, *Phys. Rev. Lett.* **88**, 097603 (2002).
- [36] K. Sokolowski-Tinten and D. von der Linde, Generation of dense electron-hole plasmas in silicon, *Phys. Rev. B* **61**, 2643 (2000).
- [37] M. Garcia-Lechuga, J. Siegel, J. Hernandez-Rueda, and J. Solis, Imaging the ultrafast Kerr effect, free carrier generation, relaxation and ablation dynamics of lithium niobate irradiated with femtosecond laser pulses, *J. Appl. Phys.* **116**, 113502 (2014).
- [38] D. H. Auston, K. P. Cheung, and P. R. Smith, Picosecond photoconducting Hertzian dipoles, *Appl. Phys. Lett.* **45**, 284 (1984).
- [39] D. Puerto, W. Gawelda, J. Siegel, J. Bonse, G. Bachelier, and J. Solis, Transient reflectivity and transmission changes during plasma formation and ablation in fused silica induced by femtosecond laser pulses, *Appl. Phys. A* **92**, 803 (2008).
- [40] M. Naftaly and A. Gregory, Terahertz and microwave optical properties of single-crystal quartz and vitreous silica and the behavior of the Boson peak, *Appl. Sci.* **11**, 6733 (2021).
- [41] G.-L. Tan, M. F. Lemon, and R. H. French, Optical properties and london dispersion forces of amorphous silica determined by vacuum ultraviolet spectroscopy and spectroscopic ellipsometry, *J. Am. Ceram. Soc.* **86**, 1885 (2003).
- [42] L. Haahr-Lillevang and P. Balling, Ultrashort-pulse laser excitation and damage of dielectric materials: Experiments and modeling, in *Pacific Rim Laser Damage 2015: Optical Materials for High-Power Lasers*, edited by J. Shao, T. Jitsuno, W. Rudolph, and M. Zhu (SPIE, Bellingham, WA, 2015).